

Simulation of Ram-Air Parachute Systems with the Panel Method and Staggered Fluid-Structure Coupling

Enrique Ortega¹, Roberto Flores¹ and Jordi Pons-Prats²

*CIMNE – Centre Internacional de Metodes Numerics en Enginyeria
Gran Capità s/n, 08034 Barcelona, Spain*

I. Introduction

THE use of numerical simulation for the analysis of parachute systems has grown considerably over the last two decades. This trend has not been driven just by the desire to reduce experimental testing costs. Numerical simulation also provides insight into the physics of the problem and detailed sets of flow and structural variables, which can be difficult to measure directly in test models. Complementing experimental testing, simulation enables more extensive and detailed studies during the early development cycle. This allows evaluation of the system's performance and reliability, as well as identification of potential problems and preemptive corrections. All these features, together with increasing computer power, promote the growing use of computer simulation in parachute design.

The first numerical tools for the analysis of parachutes date back to the early nineties. In these works, the air is modeled by potential flow and panel methods while Finite Element (FE) techniques are used for the structure. Since the discretization of the surrounding flow is not required in panel methods, the solution procedure is drastically simplified. This methodology has been applied to rigid and non-rigid ram-air configurations [1-4], and proved effective to assist in design practice, particularly with attached flow surrounding the canopy. Additional enhancements aim to improve the scope of the aerodynamic model, for example the use of empirical approximations and viscous corrections to account for the suspension lines and the real aerodynamics of canopy sections and payloads [2, 5-7]. Extensions to deal with detached flows have also been proposed. They usually solve the Lagrangian form of the Navier Stokes' momentum equation written in vorticity variables. Since only the regions of concentrated vorticity must be resolved, the parachute wake is discretized by means of point vortices while the attached (inviscid) flow areas remain mesh-free. This addresses the issue of flow separation while retaining the advantages of panel methods; see for instance [8]. Methods using potential flow aerodynamics, with different degrees of complexity and range of applications, have reached a satisfactory balance between accuracy and

¹ PostDoc Researcher, Edifici C1, Universitat Politècnica de Catalunya - Campus Nord, Gran Capità s/n 08034 Barcelona, Spain.

² Coordinator CIMNE Aerospace Group, Edifici C3, Parc Mediterrani de la Tecnologia UPC, Esteve Terrades 5, 08860 Castelldefels, Spain.

computational cost in many practical parachute problems; recent applications can be found in [9-11]. A step forward in fidelity and scope has been achieved with methods involving the solution of the Navier-Stokes equations with full discretization of the surrounding flow. These approaches have emerged mainly in the context of the **deforming-spatial-domain/stabilized space-time (DSD/SST)** methodology [12, 13], a framework which provides a general solution method for problems involving moving boundaries and interfaces. Some of the first applications, **specifically for ram-air parachutes**, can be found in [14, 15]. Later, numerous special techniques have been developed to face increasingly challenging problems. A detailed review of all these methods, applications and achievements is presented in [16], and some of the latest developments can be found in [17-19]. The literature exemplifies the capabilities of DSD/SST based techniques to deal with complex problems, such as those involved in the design of spacecraft parachutes. There are still other approaches using full discretization of the surrounding fluid. For example, a coupled Euler-Lagrange model with fabric porosity [20], a Navier-Stokes large-eddy simulation of a disk-gap-band decelerator [21], a front tracking approach for drogue parachutes [22], and applications of software packages such as LS-DYNA® to ram-air parachutes [23-26].

The simulation of parachutes is an active research line at the International Center for Numerical Methods in Engineering (CIMNE) and several tools have been developed at the request of CIMSA Ingeniería de Sistemas, a Spanish parachute manufacturer (see [27]). The developments focus mainly on the simulation of ram-air parachute systems and emphasize the cost effectiveness of the solution methodology. The objective is to obtain fast design tools, able to produce data suitable for preliminary analysis of parachute systems with minimal computational resources. The tools must also be accessible for parachute designers with a basic knowledge of computational mechanics. To meet these constraints, a low fidelity (potential) flow solver has been adopted in conjunction with staggered fluid-structure interaction coupling. The computer program developed, named PARACHUTES [28, 29], includes unsteady aerodynamic and structural calculation modules. The aerodynamics is solved with a low-order panel method and a finite element technique is used for the structure. The latter allows modeling the suspension lines, fabric and suspended payloads of a typical parachute system by means of cable, membrane and solid (3D) linear elements. The aerodynamic model is enhanced by empirical approximations to account for the drag of suspension lines, canopy and suspended payloads. The solution methodology is described in [10].

In this work, the steady flight of a ram-air parachute-payload configuration is analyzed with PARACHUTES and the results are compared with experimental data. The objective is twofold: to study the performance of the

methodology and assess its capabilities for the analysis of practical engineering problems. The numerical and experimental studies presented belong to the PARAPLANE project [30, 31] (Development of a new steerable parachute system for rescue of small and medium size airplanes), financed through the European Commission's Seventh Framework Programme.

The work is organized as follows. An overview of the analysis methodology is given in Section II. Section III deals with the reference experimental data used to evaluate the numerical simulations. The computational model employed is described in Section IV. The results obtained for the test cases are discussed in Section V and the main conclusions are outlined in Section VI.

II. Overview of the numerical methodology

The methodology implemented in PARACHUTES is reviewed below; see [10] and [32] for further details.

A. Structural modeling

The structural solution uses a large-displacement small-strain FE formulation with explicit time integration. This approach is quite accurate (only small tensile strains are expected) and allows an efficient coding. The solver models membranes, cables and solid bodies using linear elements. Since cables and membranes lack bending stiffness and buckle under compressive loads, a wrinkling model is used to correct the elemental stresses. Structural components with negligible deformation can be modeled as rigid bodies. This greatly reduces the computational cost with no effect on the structure dynamics (only 6 degrees of freedom are retained for each rigid block). The time integration is performed with an explicit second-order scheme, which despite the inherent time increment limitations, provides a robust and fast solution for highly non-linear problems. Note that the complete dynamics of the deformable parachute payload system subject to inertial, aerodynamic and gravity forces is obtained because the trajectories of all the grid points are integrated in time. A numerical dissipation model with Rayleigh damping and bulk viscosity is used to control local high-frequency modes that are not well resolved by the staggered coupling adopted. While simple and inexpensive, this model requires damping coefficients that can have a spurious effect on the results (particularly the mass-proportional damping). Some guidelines for tuning these parameters are given in [10, 29]. The code also automatically compares the energy lost by numerical damping to the work of the physical forces, so that adverse effects on the solution can be readily detected and corrected. This makes the choice of suitable damping coefficients easier. It should be noted that the dissipation forces are computed using velocities relative to the

parachute center of mass, which minimizes the effect of numerical damping on rigid-body motions. The structural solver has other interesting features, such as cable length manipulation to simulate the deflection of control lines and maneuvers. Once the required time-deformation values are provided, the solver automatically interpolates them to guarantee smooth variations (quintic splines are used).

B. Aerodynamic modeling

Potential flow aerodynamics was considered cost-effective in this work because no extensive detached flow is expected under nominal operation of gliding parachutes. Hence, the flow solution is obtained with an unsteady panel method using low-order doublets and sources. The constant strength panels lower the complexity and computational cost, while the addition of sources improves the accuracy compared to a doublet-only method [33]. Furthermore, the required discretization is simpler because exact matching between panels is not required. In order to model the wake, a time-steeping technique is used. The wake panels are shed from specified lines along the body and move following the local velocity (freestream and induced components) to account for wake rollup. The doublet strength of the panels shed into the wake is determined by enforcing the Kutta condition at the shedding lines; thus, the problem has no additional unknowns. With the time-steeping method the wake is naturally developed in a simple and inexpensive manner compared to other approaches, e.g. using wake relaxation (see [34]).

The wind loads acting on the suspension and control lines are obtained in a simplified manner, considering the cable elements as slender cylinders with specified drag coefficients. The wind forces are calculated in each element by $\mathbf{f}_i = 0.5\rho d C_d |\mathbf{v}_i| \mathbf{v}_i$ (per unit length), where ρ , d and C_d denote the air density, cable diameter and cylinder drag coefficient (based on the diameter); and \mathbf{v}_i is the transverse wind velocity (i.e. normal to the cable axis). These forces are calculated by the structural solver, meaning they are updated at each structural time increment. This method yields a reasonable approximation of the natural damping due to wind loads and does not require any additional numerical damping. This improves the accuracy of the solution and relieves the user from defining dissipation coefficients for the cables. The software also allows using aerodynamic force functions for the wind loads acting on suspended bodies. The functions can be obtained by fitting experimental data for a range of attitudes. Given the aerodynamic performance of typical payloads (cargo containers), only the drag forces are accounted for in this work. The experimental drag coefficient obtained from [35] is parameterized in terms of the body normal projected area (in the direction of the incident velocity) and the resulting force is included in the structural computation. The simplified approach used in PARACHUTES for the wind loads on the payload and suspension lines enhances the

modeling capabilities with almost no additional cost. The solver also accounts for apparent mass effects due to inertia of the air surrounding the parachute (which can affect transient behavior and stability). The additional mass is calculated with the model of Lissaman and Brown [36] and distributed across the structure nodes.

C. Coupling procedure

A 2-way staggered scheme is used to couple the aerodynamic and structural solvers, **with one fluid solve and one structure solve per time step**. Since the mesh is the same, no interpolation of results is required during the simulation. This allows obtaining both the transient and steady-state response of the structure in a very efficient way. In typical calculations, the stability limit of the structural solver is small (explicit approach), thus, several structural time increments are performed per aerodynamic step. Although this could affect the high-frequency response, it is not a serious limitation because these modes usually have low amplitude, and affect only small parts of the structure. On the contrary, the low frequency modes, which govern the overall response of the structure and are of major interest to the designer, are well resolved by the coupling scheme adopted.

D. Computational requirements

The program PARACHUTES is written in FORTRAN 90-95 language. The code has been especially designed for modularity (simple addition of new features) and low computational requirements (CPU-time and memory storage). Most of the expensive operations (e.g. the computation of the aerodynamic influence coefficients) have been parallelized using OPENMP directives. Although the methodology has been tailored for running on modest hardware platforms, it can also profit from higher performance hardware, particularly when large problems are undertaken. Typical simulation costs are given in Section V.

III. Reference experimental data

A considerable part of the software development and validation tasks presented here has been carried out in the context of PARAPLANE [30], an European research project aimed at developing a Steerable Aircraft parachute Rescue System (SARS) for small and medium airplanes up to 625 kg. The system is built-in the aircraft to be activated in case of emergency. Once deployed, an autonomous guidance unit (AGU) computes a path to a safe landing area and takes command of the parachute.

In PARAPLANE two test campaigns were conducted to determine the in-flight performance of the ram-air parachutes selected for the SARS system. The drop-tests took place at the Coolidge “Jamieson Tank” drop zone,

near MESA airport in Arizona (USA). The parachutes investigated were the CIMSA models P1 and P2. The P1 is a 900 ft² rectangular parachute for payloads up to 600 kg. The P2 has a smaller size and payload, and is equipped with slat control devices for larger brake deflection. This model was designed during the project to meet the requirements of the rescue system. The drop-units tested (Fig. 1) consisted of the parachute, the ACRIDS (Aerial Cargo RIDer System) guidance unit, and a dummy payload. During the tests, the drop altitude was set to 10,000 ft MSL and the airdrops were driven by gravity. Right after the deployment, pre-planned maneuvers were executed by remote control at high altitude to obtain data for aerodynamic characterization. Next, the autonomous control was engaged to test the automatic landing capability. Fully autonomous flights were also carried out satisfactorily.

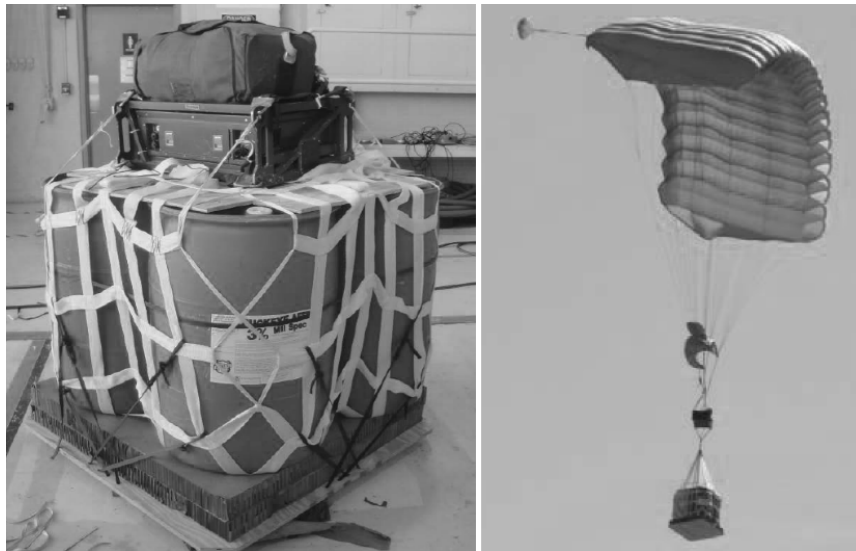


Fig. 1. PARAPLANE drop-unit (left). In-flight view of the system equipped with the P1 parachute (right).

This paper focuses on the study of the parachute steady descent velocity and glide ratio for different deflections of the steering lines. The reference experimental values used were obtained from GPS data, time-averaging the values taken during the steady part of the flight (approximately at constant sink of rate). The test data were corrected to standard sea-level conditions (with no compensation for wind or other weather effects). Reliable uncertainty estimates for the experimental data were not available to the authors during the preparation of this work.

IV. Numerical test model

The parachute model CIMSA P1 is used in this work because a higher amount of reliable test data was available. The model discretization and problem setup employed in the simulations are described below.

A. Model discretization

The computational model was constructed from the original layout of canopy fabric panels and suspension lines, and a simplified representation of the AGU and the payload is used (they are assumed rigid and its aerodynamics is obtained from empirical data). A view of the model is given in Fig. 2. This is the undeformed configuration used to start the simulations. Since the deployment and inflation phases are not calculated, the simulated and experimental results are not comparable until the system approaches cruise conditions.



Fig. 2. Undeformed model configuration (CIMS P1 parachute, AGU and payload).

The computational model is discretized using linear 2-node cables, 3-node membranes and 4-node tetrahedral elements. The cable elements are used for the suspension lines and canopy seams and reinforcement tapes, while membrane elements model the canopy fabric. Solid tetrahedral elements are used for the AGU and the payload. Since the deformation of these two components is not relevant to the test cases studied, they are simulated as rigid bodies to reduce the computational cost (only 12 degrees of freedom are retained). Only the elements belonging to the external surface of the canopy (those exposed to the wind) are processed by the aerodynamic solver. The wind forces acting on the rest of elements are modeled using empirical correlations (see Section II-B). The canopy is originally meshed with quadrilateral aerodynamic panels (which behave better than the triangular), and these elements are then automatically split into 3-node triangles when solving the structure. The discrete model has 19324 nodes and 30896 elements (8811 cables, 10842 triangles, 10281 quadrilaterals and 962 tetrahedra).

The mechanical properties of the materials used for the canopy and suspension lines are those of the real parachute provided by the manufacturer. Since the AGU and the payload are considered rigid, uniform densities matching the actual mass of the component are assumed.

B. Problem setup and parameters calibration

In order to obtain the steady descent characteristics of the parachute system, the simulations are started with the undeformed model and continue until the equilibrium flight configuration is reached. The model is released with an initial velocity with the atmosphere at rest. Due to the unsteadiness of the problem, the steady flight condition is determined in an approximated manner (total system acceleration below a given threshold). Some amount of under-relaxation is applied when updating the aerodynamic forces to reach the equilibrium condition faster. In the test cases involving pulls on the steering lines, these are input as a series of time vs. deformation (% shrink) values.

Among the parameters needed for the structural computation, the numerical dissipation coefficients require special attention. Remember that numerical damping is only necessary for the canopy membrane elements as the wind loads introduce a natural damping mechanism on the suspension lines. The damping coefficients applied to the different materials have been set to the minimum necessary for stability, avoiding negative effects on the structure dynamics. To this end, the dissipation forces are calculated using velocities relative to the system's center of mass and the magnitude of the net viscous forces introduced is always checked *a posteriori*. Some additional damping is also applied during the initial steps to accelerate the convergence to cruise conditions. Since the deployment and inflation stages are not modeled, the problem initial conditions may be unrealistic (initial velocity and attitude are often incorrect). This approach works well because the canopy undeformed geometry (obtained from the manufacturing patterns) is not too far off from its flight configuration. In other cases, pre-calculated deformed geometries may be necessary to start the simulations; suitable methods are reviewed in [16].

The aerodynamic solver only processes the external canopy surfaces, but the lateral stabilizers are removed from the aerodynamic model because preliminary tests have shown no significant effects. This reduces the possibility of wake-canopy panels intersection and the computational cost. The flow inside the canopy cells is not resolved by the program, and only a constant stagnation pressure is applied inside the canopy to keep it pressurized (as discussed later, this assumption can introduce some error in the canopy axial force). Although the air intakes must be meshed to obtain the closed shape required by the flow solver, these panels must not interfere with the structural behavior (both aerodynamic and structural models share the same mesh). To this end, no aerodynamic load is applied on

intake panels and they are assigned a very small thickness and Young's modulus. This makes the mass and load bearing capability of the inlet panels negligible compared to the rest of canopy, thus approximating an open inlet.

As described in Section II-B, empirical drag coefficients are used to calculate the wind loads on the suspension lines. These values are obtained from experiments for slender cylinders in transverse flow. For the present test cases the expected Reynolds numbers vary between 2000 and 5000 (based on the cable diameters); thus, the drag coefficient to be applied is $C_d \approx 1$ [37]. However, since the suspension lines in the wake of other cables are subject to lower dynamic pressures and drag forces, this value should be reduced. The final value applied is $C_d=0.8$, and it is adjusted using experimental data from similar configurations. Regarding the parachute canopy, some drag is also added to achieve a more realistic behavior. This is carried out by prescribing a constant (fictitious) drag coefficient for the line elements modeling the canopy reinforcements and seams. Since these elements are processed similarly to the suspension lines, this is a way of introducing the canopy viscous drag without making changes in the code. The fictitious drag coefficient applied to the canopy reinforcements is $C_d=0.6$. This value has been determined by matching the total drag of the canopy and the suspension lines to the zero-lift drag of the system. The latter was provided by the manufacturer, but typical parachute drag-breakdowns or information about the flight path slope (with no control deflection) can be also used if specific data is not available, see [38]. The aerodynamic drag of the payload and the AGU are also calculated using empirical force functions (only drag forces are considered). These are obtained in terms of the projected frontal area of the bodies by fitting the data given in [35]. Additional details on the calibration of the model parameters are provided in Section V-C.

V. Test cases

The steady descent flight of the system is studied here with and without deflection of the steering lines. The test case with no deflection is presented first, and the same configuration is then solved for symmetrical control lines deflections ranging between 15 and 80% of the full servo stroke (130 cm). The results are compared with test measurements to assess the capabilities of the solution technique. It is important to note that the discrete model, material properties and numerical parameters are the same for all the test cases presented. The adjustment was performed only once for the steady flight configuration without control lines deflection, with the same settings used for the different maneuvers simulated.

A. Case 1: free-flight without steering line deflection

The simulation of the equilibrium descent of the system without pulling the steering lines is started by releasing the model with no initial velocity and no wind (standard sea-level conditions are used). The equilibrium condition is reached 30 seconds after release. Fig. 3 shows the time history of the total horizontal (HH) and vertical (VV) accelerations of the system center-of-mass. The evolution of the horizontal (HFV) and descent (DFV) flight velocities and the glide-slope angle (measured from the horizontal) is presented in Fig. 4.

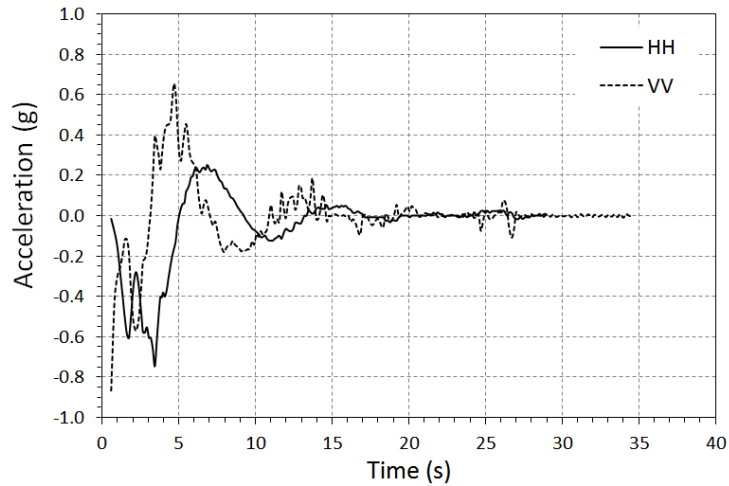


Fig. 3. Calculated time evolution of the vertical (VV) and horizontal (HH) accelerations of the system.

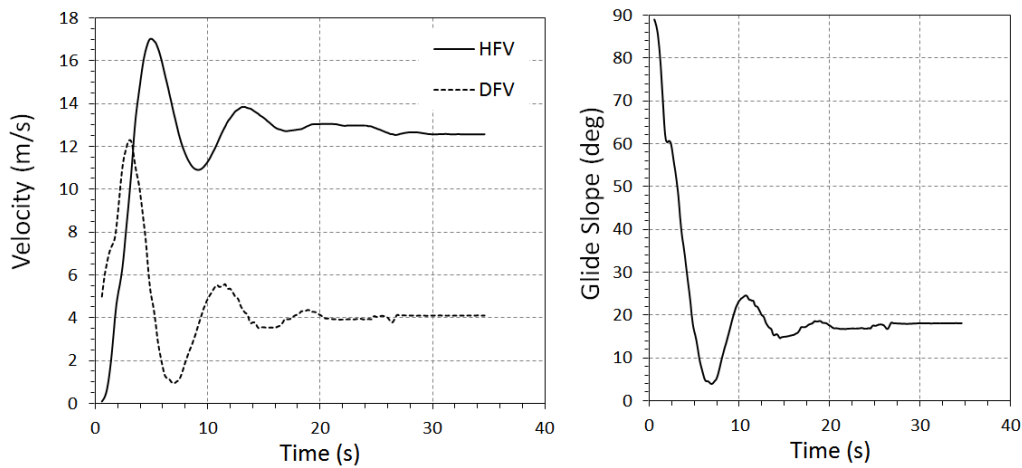


Fig. 4. Calculated time evolution of the horizontal (HFV) and descent (DFV) flight velocities and glide-slope.

The steady flight velocities are compared with experimental values in Table 1. The difference in the prediction of the glide-slope is about 14%, which is satisfactory in view of the complexity of the problem. The descent velocity shows a larger discrepancy, especially the vertical component. The possible causes are discussed below.

	PARACHUTES	TEST	DIFFERENCE (%)
Horizontal flight velocity (HFV m/s)	12.5	14.5	-14%
Descent flight velocity (DFV m/s)	4.1	5.6	-27%
Glide slope (deg)	18.2	21.1	-14%

Table 1. Comparison of numerical and experimental results.

The global lift and drag coefficients derived from the experimental data are **CL=0.4** and **CD=0.15** respectively. Regarding lift, the simulation yields **CL=0.53**. An increase of lift is expected because the potential solver does not account for viscous effects such as boundary layer thickening and detachment, which tend to reduce the lift for the same attitude and flight conditions. In addition, there were some uncertainties in the model geometry due to detailed data not being disclosed. This affected in particular the length of the suspension lines which controls the rigging angle of the canopy and, in turn, the equilibrium angle of attack. This can have a large impact in the global lift coefficient and no experimental measurement of the canopy incidence was available for cross-check. The excess of CL is largely responsible for the lower steady flight velocity observed in the simulation. Concerning the drag coefficient, the value obtained is **CD=0.17**, slightly higher than the experimental result. The difference can be due to factors such as the higher lift developed by the model (causing additional induced drag), the contribution of the canopy internal pressure (which produces a net force as explained below), and uncertainties in the estimation of the viscous drag (recall that only the parasitic drag was adjusted in this example). Since the last two factors are presumably the most relevant, additional experimental data and improved drag models (e.g. accounting for interference between structural elements and flow separation) could help to enhance the numerical results. It is important to note that since the canopy structurally behaves as an open body, the internal pressure generates a net force oriented mainly in the chord direction (due to the air inlets). This contribution to the drag force is overestimated in the simulation because the real average inflation pressure should be below the stagnation value (there is internal flow between cells and across the fabric). The excess drag also contributed to a reduced flight velocity (but to a lesser degree than the error in lift). As the relative excess of lift is larger than the drag increase in the computations, the net result is a predicted flight path angle shallower than the experimental value. Note that the error in drag can also change the equilibrium angle of attack of the canopy (by moving it rearwards) and, thus, the global lift. Altogether, taking into account the existing uncertainties in the flight test data (for which no reliable estimates are available), the model geometry and the materials characterization, the results are deemed satisfactory. Fig. 5 shows some views of the calculated steady flight configuration.



Fig. 5. Views of the calculated parachute-payload system in steady flight.

Regarding computational requirements, the CPU-time required to simulate one second in this example was about 34 minutes and the memory storage needed 1 Gb. The simulation was performed on two-CPU board featuring Intel Xeon E5645 processors @ 2.4 GHz (12 Mb L2 cache) running on 6 cores. Although the computational cost can vary depending on the problem setup, this example shows that many useful structural and flow data can be obtained with this methodology in reasonable times and modest hardware resources.

B. Case 2: symmetrical deflection of the steering lines

The steady descent of the parachute system is now investigated for symmetrical deflection of the steering lines. The model and problem setting are maintained, but in this case the undeformed configuration (Fig. 2) is released with the steady flight speed calculated in the previous case. The desired line deflection is applied immediately after the release, and the simulation continues until the equilibrium flight configuration is reached. The cases studied involve deflections of 15, 30, 60 and 80% of the full servo stroke (130 cm).

The equilibrium flight velocities calculated for the various deflections of control lines are shown in Fig 6 (left) along with the test values. The experimental trend is well captured by the numerical solution and the agreement observed for deflections of 30, 60 and 80% is satisfactory. As in the previous case, the magnitude of the calculated velocities is generally lower. It can be also noted that the numerical results show no significant variations for deflections below 30%. This may be due to some slack of the control lines having been removed from the experimental setup during assembly. In any case, notice that very small changes are also observed in the test data

measured for the same range of deflection (particularly the descent velocity). Although the results are not shown here, it was found that simulations with larger control deflections (100% and higher) produced highly inaccurate results. In such cases, the large curvature of the canopy near the trailing edge causes extensive detached flow and a loss of command effectiveness, viscous phenomena that cannot be reproduced in an inviscid solution. Concerning the glide slope, only slight variations are observed in both experimental and numerical results. As in the previous case, the predicted glide angle is about 10% lower than the measured value.

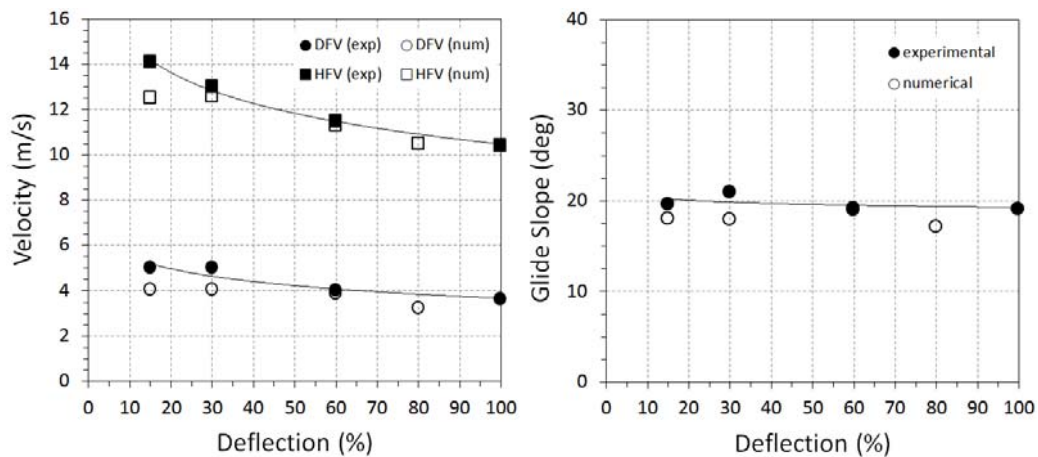


Fig 6. Calculated and experimental results for symmetrical deflection of the steering lines. Left: steady horizontal (HFV) and descent (DFV) flight velocities. Right: glide slope (the solid lines indicate the trend of the experimental data).

A comparison of equilibrium lift and drag coefficients is presented in Fig 7. Again, no significant variation is observed for deflections below 30%. For larger deflections, the computed lift closely follows the experimental trend. The differences observed for the drag are small up to a 60% deflection, but the experimental trend is not reproduced beyond that point (the calculated drag becomes almost constant). Note that the parasitic separation drag, which plays an increasingly important role at larger deflections, is not reproduced with the current methodology.

Finally, snapshots of the computed steady flight configurations are shown in Fig. 8 and Fig. 9. The curvature of the canopy near the trailing edge becomes sharper with increasing control line deflection (at the same time, the point at which the kink on the surface develops tends to move backwards). This abrupt change in geometry causes a massive flow separation in the real flow, but the model cannot reproduce it due to its inviscid character. Hence, the maximum deflection was limited to 80% of full the servo stroke (i.e. 104 cm).

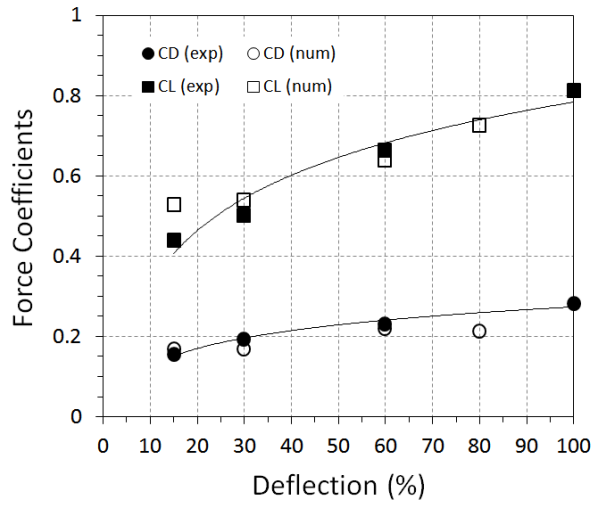


Fig 7. Calculated and experimental aerodynamic force coefficients for symmetrical deflection of the steering lines (the solid lines indicate the trend of the experimental data).

It is interesting to note that the simulations revealed a small tendency of the system to yaw (without rolling) to the right. Although the side displacement is almost negligible for small deflections, the effect becomes more evident for larger deflections. Some small asymmetry in the model cannot be discarded, but it is also possible that the flow unsteadiness (caused by the canopy deformation) could induce a yaw movement not counteracted by the parachute in a natural manner, leading to a small directional instability. Based on these results, the action of the parachute lateral stabilizers should be re-examined (these were not simulated in the present study, see Section IV-A).

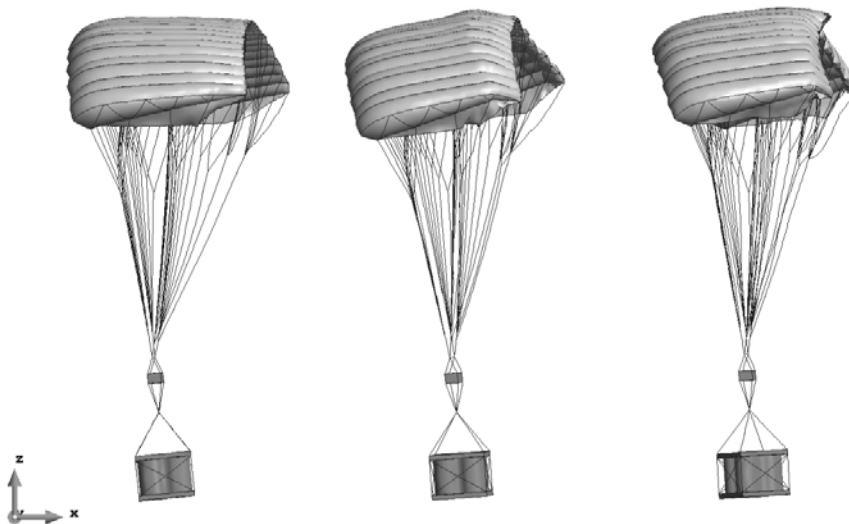


Fig. 8. Lateral view of the steady system configuration calculated for symmetrical deflection of the steering lines. From left to right: 30, 60 and 80% line deflection.

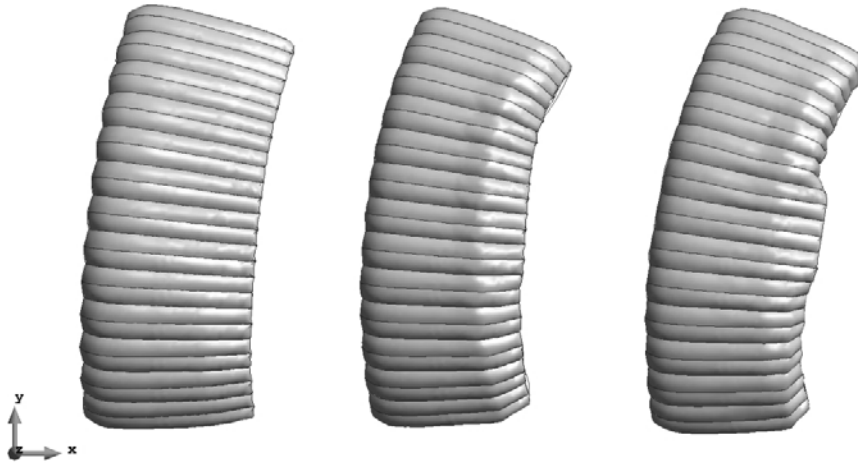


Fig. 9. Plan view of the steady system configuration calculated for symmetrical deflection of the steering lines. From left to right: 30, 60 and 80% line deflection.

C. Remarks on the choice of model parameters

Since the geometry, mechanical properties and mass distribution of the system are taken from the real parachute, the only free parameters in the model are the coefficients of parasitic drag (suspension lines and canopy) and damping (canopy fabric). To determine suitable drag coefficients, the cable drag is first chosen based on experimental data (see section IV-B). Next, the parasitic canopy drag is adjusted until the total zero-lift drag of the parachute provided by the manufacturer is matched. The effects of drag distribution between the cables and canopy have been not investigated because they would require experimental data not available to the authors. Concerning canopy damping, it is important to stress that it is added to suppress local spurious oscillations and to make the simulation proceed smoothly. In this work, several numerical experiments were performed following [10, 29] to determine the minimum values required. It was verified that the resulting net damping forces and moments (this information is provided by the simulation code) are at least two orders of magnitude smaller than the inertial, aerodynamic and elastic forces. Hence, the expected effect on the global response of the system (e.g. trajectory) is small. Given that PARACHUTES was designed as a low fidelity tool optimized for speed, the compromises made are considered acceptable.

As mentioned before, the damping and drag coefficients were adjusted only once for the steady flight condition without control lines deflection, and the values retained for all the cases involving maneuvers. In fact, the deflection in the analyses was limited to 80% because the drag coefficients adjusted for smooth flow conditions cannot reflect the increase in parasitic drag due to extensive flow separation (the potential solution also lacks reliability in such

cases). The results presented are thus representative of the accuracy that can be achieved over most of the flight envelope using a single reference condition to calibrate the model parameters.

VI. Conclusion

A cost-effective low-fidelity method for the simulation of ram-air parachute-payload systems has been presented. It is based on a panel potential flow solver and staggered fluid-structure interaction coupling. The test cases presented analyze the descent of a parachute-payload configuration with and without deflection of the steering lines. Placing the focus on the validation of steady descent velocities and glide ratios, the simulations showed satisfactory results for the range of conditions investigated.

The study also revealed the need to improve some aspects of the methodology, in particular those related to the estimation of the viscous drag contributions. In this regard, improved semi-empirical models accounting for separation drag effects could help to enhance the modeling with little additional cost. Improved estimates are also needed for a better representation of the canopy internal flow (which affects the total drag), and the permeability of the fabric can be simulated with simple code modifications using transpiration velocities. Overall, the results obtained are very encouraging and show that useful data for the practical analysis of parachutes can be obtained with simplified models and affordable computational costs.

Acknowledgments

The authors would like to acknowledge the financial support provided by the PARAPLANE project under the European Commission's Seventh Framework Programme (contract number SME-2012-1-315105). Special thanks to CIMSA Ingeniería en Sistemas and the PARAPLANE consortium for providing the models, test data and many useful inputs during the development of this work.

References

1. Chatzikonstantinou, T., *Numerical analysis of three-dimensional non rigid wings*. AIAA paper 89-0907, Aerodynamic Decelerator Systems Technology Conference, 10 th, Cocoa Beach, FL, 1989.
2. Ross, J.C., *Computational Aerodynamics in the Design and Analysis of Ram-Air-Inflated Wings*. AIAA Paper 1991-1548, 1993: p. 10-13.
3. Chatzikonstantinou, T., *Recent advances in the numerical analysis of ram air wings - The three dimensional simulation code 'PARA3D'*. 12th Aerodynamic Decelerator Systems Technology Conference, 1993.
4. Chatzikonstantinou, T., *Problems in ram air wing modeling and their solution in the three dimensional simulation code 'PARA3D'*. 15th Aerodynamic Decelerator Systems Technology Conference, Aerodynamic Decelerator Systems Technology Conferences, paper AIAA-99-1716, 1999.

5. Mittal, S., Saxena, P., and Singh, A., *Computation of two-dimensional flows past ram-air parachutes*. International journal for numerical methods in fluids, 2001. **35**(6): p. 643-667.
6. Balaji, R., Mittal, S., and Rai, A.K., *Effect of leading edge cut on the aerodynamics of ram-air parachutes*. International Journal for Numerical Methods in Fluids, 2005. **47**(1): p. 1-17.
7. Mohammadi, M.A. and Johari, H., *Computation of Flow over a High Performance Parafoil*. 20th AIAA Aerodynamic Decelerator Systems Technology Conference and Seminar, paper AIAA 2009-2979, 2009.
8. Strickland, J.H., Homicz, G.F., Porter, V.L., and Gossler, A.A., *VIPAR version 1.0*. SANDIA report SAND2002-2174, 2002.
9. Altmann, H., *Numerical simulation of parafoil aerodynamics and dynamic behaviour*. In 20th AIAA Aerodynamic Decelerator Systems Technology Conference and Seminar, Seattle, WA, USA, paper AIAA 2009-2947, 2009.
10. Flores, R., Ortega, E., Onate, E., *Simple and efficient numerical tools for the analysis of parachutes*. Engineering Computations, 2014. **31**(5).
11. Altmann, H., *Fluid-Structure Interaction Analysis of Ram-Air Parafoil Wings*. 23rd AIAA Aerodynamic Decelerator Systems Technology Conference, paper AIAA 2015-2184 2015.
12. Tezduyar, T.E., Behr, M., Mittal, S., and Liou, J., *A new strategy for finite element computations involving moving boundaries and interfaces-the deforming-spatial-domain/space-time procedure: II. Computation of free-surface flows, two-liquid flows, and flows with drifting cylinders*. Computer Methods in Applied Mechanics and Engineering, 1992. **94**(3): p. 353-371.
13. Tezduyar, T.E., Behr, M., and Liou, J., *A new strategy for finite element computations involving moving boundaries and interfaces: the deforming-spatial-domain/space time procedure: I. The concept and the preliminary numerical tests*. Computer Methods in Applied Mechanics and Engineering, 1992. **94**(3): p. 339-351.
14. Kalro, V., Aliabadi, S., Garrard, W., Tezduyar, T., Mittal, S., Stein, K., *Parallel finite element simulation of large ram-air parachutes*. International Journal for Numerical Methods in Fluids, 1997. **24**(12): p. 1353-1369.
15. Kalro, V., Tezduyar, T., *A parallel 3D computational method for fluid-structure interactions in parachute systems*. Computer Methods in Applied Mechanics and Engineering, 2000. **190**(3-4): p. 321-332.
16. Takizawa, K. and Tezduyar, T., *Computational methods for parachute fluid-structure interactions*. Archives in Computational Methods in Engineering, 2012. **19**: p. 125-169.
17. Takizawa, K., Matthew Fritze, M., Montes, D., Spielman, T., and Tezduyar, T., *Fluid-structure interaction modeling of ringsail parachutes with disreefing and modified geometric porosity*. Computational Mechanics, 2012. **50**(6): p. 835-854.
18. Takizawa, K., Tezduyar, T., Boswell, C., Tsutsui, Y., and K., M., *Special methods for aerodynamic-moment calculations from parachute FSI modeling*. Computational Mechanics, 2015. **55**(6): p. 1059-1069.
19. Takizawa, K., Tezduyar, T., and Kolesar, R., *FSI modeling of the Orion spacecraft drogue parachutes*. Computational Mechanics, 2015. **55**(6): p. 1167-1179.
20. Aquelet, N. and Tutt, B., *A new fluid structure coupling application to parachute modelling*. European Journal of Computational Mechanics/Revue Européenne de Mécanique Numérique, 2007. **16**(3-4): p. 521-536.
21. Karagiozis, K., Kamakoti R., Cirak, F., and Pantano, C., *A computational study of supersonic disk-gap-band parachutes using Large-Eddy Simulation coupled to a structural membrane*. Journal of Fluids and Structures, 2011. **27**: p. 175-192.
22. Kim, J.-D., Li, Y., and Li, X., *Simulation of parachute FSI using the front tracking method*. Journal of Fluids and Structures, 2013. **37**: p. 100-119.
23. Ibos, C., Lacroix, C., Goy, A., and Bordenave, P., *Fluid-structure simulation of a 3D ram air parachute with SINPA software*. 15th Aerodynamic Decelerator Systems Technology Conference, paper AIAA-99-1713, 1999.
24. Oye, I.J., *Development of Aerodynamic Analysis Software Tools within the FASTWing CL Project*. 20th AIAA Aerodynamic Decelerator Systems Technology Conference and Seminar, Seattle, WA, USA paper AIAA 2009-2931, 2009.
25. Tutt, B., Richard, C., Roland, S., and Noetscher, G., *Development of parachute simulation techniques in LS-DYNA*, in *11th International LS-DYNA Users conference 2010*: Detroit.
26. Y. Coquet Y., Bordenave, P., Capmas, G., and Espinosa, C., *Improvements in Fluid Structure Interaction Simulations of Parachutes Using LS-Dyna®*. 21st AIAA Aerodynamic Decelerator Systems Technology Conference and Seminar, Dublin, Ireland, paper AIAA 2011-2590, 2011.
27. *CIMSA Ingeniería en Sistemas*. Web page: <http://www.cimsa.com/> (August 2015).
28. Ortega, E. and Flores, R., *PARACHUTES. A computer program for calculating ram-air parachutes. Theory document*. CIMNE publication, 2015.
29. De la Torre, D., Ortega, E., and Flores, R., *PARACHUTES. A computer program for calculating ram-air parachutes. User's manual*. CIMNE publication, 2015.
30. *PARAPLANE*. Web page: <http://www.cimne.com/paraplane>, CIMNE 2015.
31. *PARAPLANE. Development of a New Steerable Parachute System for Rescue of Small and Medium Size Airplanes. REF. 315105- Seventh Framework Program, European Comission, 01/12/2012 - 30/06/2015*.
32. Flores, R., Ortega, E., Valles, J., Oñate, E. *A simulation tool for parachute/payload systems*. in *11th World Congress on Computational Mechanics (WCCM XI)*. 2014. Barcelona, Spain.

33. Ashby, D.L., *Potential flow theory and operation guide for the panel code PMARC_14*. NASA TM-1999-209582, 1999.
34. Maskew, B., *Program VSAERO theory document. A computer program for calculating nonlinear aerodynamic characteristics of arbitrary configurations*. NASA Report 4023, 1987.
35. Cicolani, L., Kanning, G., *A comprehensive estimate of the static aerodynamic forces and moments of the 8- by 8- by 20-Foot cargo container*. NASA Technical Memorandum 89433, 1987.
36. Lissaman, P., Brown, G., *Apparent mass effects on parafoil dynamics*. AIAA Paper 1993-1236, 1993: p. 10-13.
37. Hoerner, S.F., *Fluid-dynamic drag: practical information on aerodynamic drag and hydrodynamic resistance* 1965: Midland Park, NJ: Hoerner Fluid Dynamics.
38. Lingard, J., *Precision aerial delivery/ram-air parachute design*. 13th AIAA ADS Conference and Seminar, Clearwater Beach, 1995.